JOURNAL OF PROPULSION AND POWER
Vol. 13, No. 5, September–October 1997

Comparison of Scramjet Engine Performance in Mach 6 Vitiated and Storage-Heated Air

Tohru Mitani,* Tetsuo Hiraiwa,† Shigeru Sato,‡ Sadatake Tomioka,† Takeshi Kanda,§ and Kouichiro Tani‡
National Aerospace Laboratory, 1 Kimigaya, Kakuda, Miyagi 981-15, Japan

To investigate the sensitivity of combustion to the test gas, an H_2-fueled scramjet engine was tested at a Mach 6 flight condition with the air supplied by a combustion heater (*V* mode) and a storage heater (*S* mode). The fuel self-ignited without the assistance of igniters in the *V* mode. However, self-ignition was difficult in the *S* mode. The easier ignition with vitiated air was caused by radicals supplied from the combustion heater. The combustion behavior was also affected by the test air, which suggests that the combustion was not fully mixing-controlled. As the fuel flow rate increased, the combustion changed from a weak mode, delivering a lower thrust, to an intensive mode, with a higher thrust. Gas sampling showed that the weak combustion was caused by autoignition in the boundary layer on the engine walls. In the intensive combustion mode, the flame was anchored near the backward-facing step on the sidewalls. However, the flame partially detached from the step on the top wall in the combustor. The detached flame may make the combustion kinetically controlled to produce the sensitivity to the test air.

I. Introduction

HYPERSONIC wind tunnels require high-temperature test air to simulate scramjet inlet or combustor inlet conditions. Several different types of heaters, including arc heaters, combustion heaters, thermal storage heaters, and shock tunnels, are used at various facilities to generate test gas. The test gas generated in each of these facilities can be contaminated with different species that may have effects on the resulting combustion. Many numerical works have reported the effect of vitiated air via H_2O and radicals[1–8]; however, few experimental works have reported on the sensitivity of scramjet performance. Only one datum on air source is reported.[9] Guy et al.[9] report that the thrust in the arc-heated air is significantly higher than in the *V* mode. The program should progress to determine the sensitivity of scramjet combustion to the test gas source.[7]

The National Aerospace Laboratory of Japan has constructed a RamJet Engine Test Facility (RJTF),[10] which can simulate flight conditions of M4, M6, and M8. Hydrogen-fueled scramjet engines have been tested using RJTF.[11–16] A unique feature of the RJTF is that one may choose either a storage air heater (SAH, *S* mode) or a vitiation air heater (VAH, *V* mode) for the M6 condition, to raise the air temperature to 1500 K. Comparison of test results using these two heating sources can reveal the vitiation effect caused by VAH, and provide a basis for the M8 testing, in which the VAH has to be employed together with the SAH to produce the high-temperature air of 2600 K. The study of the facility sensitivity was initiated using the RJTF, and some of the comparative study is presented here.

Presented as Paper 96-4555 at the AIAA 7th International Space Planes and Hypersonic Systems and Technologies Conference, Norfolk, VA, Nov. 18–22, 1996; received Dec. 6, 1996; revision received April 8, 1997; accepted for publication April 16, 1997.

*Head, Ramjet Combustion Section, Kakuda Research Center. Member AIAA.

†Researcher, Ramjet Combustion Section, Kakuda Research Center. Member AIAA.

‡Senior Researcher, Ramjet Performance Section, Kakuda Research Center. Member AIAA.

§Senior Researcher, Ramjet Structure Section, Kakuda Research Center. Member AIAA.

II. RJTF, Engine, and Measurements

A. Combustion Heater and Test Air

The *S*-mode air is supplied by the SAH, which can deliver up to 29.5 kg/s of heated air at pressures up to 12 MPa. A concentric, cored brick design was adopted because this provides lower dust contamination to the test air and minimizes bed flotation concerns. The bed of the SAH is 1124 mm in diameter and 6096 mm high, and consists of five concentric cylinders of high-density, high-purity aluminum oxide, cored bricks. The pressure vessel is 1776 mm in diameter and 9905 mm high. A high-temperature valve is utilized at the outlet of the SAH to control the hot and high-pressure airflow.

The *V*-mode air is provided by the H_2–O_2–air VAH, installed upstream of the M6 facility nozzle. The M6–VAH is 267 mm in diameter and 1960 mm in length. For testing, the burner is controlled to supply oxygen-replenished combustion products containing 21% O_2. The test air is expanded through a two-dimensional-contoured supersonic nozzle. Pitot pressure surveys of the core flow in the calibration tests show $M = 5.15 \pm 0.15$ with $T_0 = 1405 \pm 40$ K for the *V* mode, and $M = 5.30 \pm 0.1$ with $T_0 = 1450 \pm 50$ K for the *S* mode at the nozzle exit.[10] The complete combustion of H_2 supplied to the VAH was confirmed by gas sampling in the calibration testing.

The chemical equilibrium calculations show the condition of test air supplied from the VAH and the SAH in Table 1, in which the chemical compositions are assumed to freeze at the nozzle throats in the frozen case. Table 1 shows that there are no significant differences between two testing media, except the specific heats. The vitiated air has a 9.5% larger specific heat than the *S*-mode air because it contains 17.7% of H_2O. The other major difference is that the vitiated air contains radicals. The radicals may freeze in the facility nozzle to be ingested by the engine. The 80 ppm of OH found in Table 1 does not reflect the actual reactive flow in the VAH as a diffusion-type combustor. The real radical concentration is expected to be much higher than that found in Table 1. Chemical kinetic calculations developed for a scramjet nozzle study[16] showed no significant amounts of nitric compounds, except for NO in the test air prepared for engine testing.

B. Scramjet Engine

The scramjet engine tested in the present study is a rectangular engine with a length of 2.1 m, as shown in Fig. 1. Details are found in Ref. 12. It consists of the cowl, the top wall, and

Table 1 Comparison of the test air

	M6 vitiation		M6 storage	
	Equilibrium	Frozen	Equilibrium	Frozen
T_0, K	1581	1581	1612	1612
P_0, MPa	46.4	46.4	47.4	47.4
m_{air}, kg/s	22.8	——	29.6	——
m_{H_2}, kg/s	0.363	——	0	——
m_{O_2}, kg/s	4.43	——	0	——
Conditions at facility nozzle exit (ε = 37.04)				
T_s, K	294	292	273	272
Ps, kPa	5.99	5.98	5.67	5.66
Mach no.	5.092	5.095	5.241	5.246
Velocity, m/s	1796	1793	1738	1735
H_2O, mole	17.7	17.7	0	0
OH, ppm	0	80	0	0
NO_x, ppm	0	1675	0	2270
c_P	0.263	0.263	0.240	0.240
γ	1.385	1.385	1.4	1.4

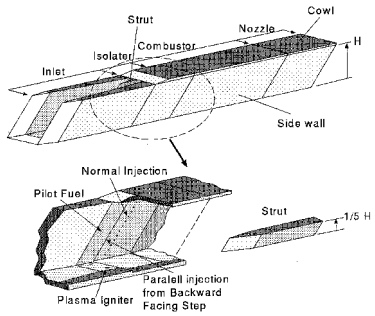

Fig. 1 H_2-fueled scramjet engine used in this study (units in millimeters).

two sidewalls. The entrance and the exit of the engine are 200 mm wide by 250 mm high (denoted by H). The engine is an uncooled, heat-sink type made of copper. The leading edges, which are exposed to severe heating, are made of nickel.

The inlet is a sidewall-compression-type with a 6-deg half-angle. The leading edge is swept back by 45 deg to deflect the airstream for spillage required in starting. The geometrical contraction ratio is 2.86 without struts. Two kinds of struts are prepared: a 50-mm-high ($1/5H$) strut and a 250-mm-high ($5/5H$) strut. In most of the present study, the $1/5H$ strut was attached on the top wall of an engine isolator between the inlet and the combustor. There was no fuel injection from the strut.

To reduce the inlet/combustor interaction, the constant area isolator was placed between them. Performance of the engine was examined using two kinds of isolators with lengths of 100 and 200 mm. The engine had two 2.5-kW plasma jet (PJ) igniters. Backward-facing steps between the isolator and the combustor were adopted for flameholding. Their heights were 4 mm on the sidewalls and 2 mm on the top wall.

The main H_2 was injected vertically from the sidewalls through 24 holes, or tangentially to the sidewalls through 24 holes (1.5 mm in diameter) on the steps. Three fuel-control systems, each consisting of three sets of solenoid valves and orifices, were prepared in independent fuel supply lines to change the H_2 flow rate during one experimental run. We programmed the fuel flow rates to eight preset values by changing the combinations of the orifices during a typical testing duration of 15 s.

C. Measurements and Procedure

We measured thrust, lift, and pitching moment delivered by the engine by a floating-frame force measuring system (FMS). We conducted engine tests without clamping the FMS throughout wind-tunnel operation. Therefore, the engine drag can be measured with comparisons with/without the airflow. Then H_2 fuel was injected in the engine. The difference between forces with/without fuel corresponds to the thrust delivered with combustion. The increment from the baseline with the airflow (the engine drag) is defined as the net thrust.

We also measured the wall pressure at 150 stations to evaluate thrust obtained by the pressure integration. The pressure thrust was compared with the thrust measured using the FMS to estimate the friction drag on the engine. We found a good correlation between the two thrusts. However, the accuracy of lift and pitching moment evaluated by the pressure integration was poor because the number of pressure sensors is limited on the top and on the cowl walls.[11] The friction drag was estimated to occupy about one-half of the total engine drag in our Mach 6 testing.

Pitot pressure and gas sample measurements were made 5 mm downstream of the engine nozzle exit with three water-cooled, 12-probe rakes. The design of the raked probes is similar to those employed by Anderson et al.[17] and Chinzei et al.[18] for supersonic combustor studies. We chose a tip passage diameter of 0.6 mm following a sudden expansion to freeze chemical reactions in the probes. Gas samples were collected in 40-cc bottles for 1.4 s, and a gas chromatography was used to measure the amount of H_2, O_2, and N_2. The local equivalence ratio Φ and the local combustion efficiency η_c are calculated with X_{O_2}/X_{N_2}, X_{H_2}/X_{N_2} in the sampled gas, and $(X_{O_2}/X_{N_2})_0$ in the air supplied to the engine, where X_i denotes the mole fraction of species i. The equivalence ratio and the combustion efficiency are given by the following equations[18]:

$$\Phi = 1 + \left[\frac{1}{2}\left(\frac{X_{H_2}}{X_{N_2}}\right) - \left(\frac{X_{O_2}}{X_{N_2}}\right)\right] \cdot \left(\frac{X_{N_2}}{X_{O_2}}\right)_0 \tag{1}$$

$$\eta_c = \begin{cases} \left[1 - \left(\dfrac{X_{O_2}}{X_{N_2}}\right) \cdot \left(\dfrac{X_{N_2}}{X_{O_2}}\right)_0\right] \Big/ \Phi & \text{for} \quad \Phi \le 1 \qquad (2) \\ 1 - \left(\dfrac{X_{O_2}}{X_{N_2}}\right) \cdot \left(\dfrac{X_{N_2}}{X_{O_2}}\right)_0 & \text{for} \quad \Phi > 1 \qquad (3) \end{cases}$$

Gas sampling is based on the assumption that gas composition is preserved in the sampling process. However, preservation of major species becomes difficult under this scramjet testing condition. The possibility of freezing the chemical reaction in probes is still controversial.[17,19–21] Criteria of chemical quenching in gas sampling is discussed for methane-fueled ramjet engines and H_2-fueled scramjet engines.[22]

We repeated two experiments to obtain the distributions of pitot pressure and gas compositions at 66 stations on the exit plane of the engine. In addition to the measurement during engine operation, we measured pitot pressures without fuel injection to investigate the interaction of combustion to the flowfield inside the engine.

III. Combustion in *V* and *S* Modes

A. Ignition and Flameholding

Because qualitative features of ignition and flameholding did not change with any engine configurations, the results on the

Table 2 Comparison of combustion properties

Testing air modes	Storage	Vitiation
Autoignition without preheating	Impossible	Possible
Autoignition with preheating	Marginal	Possible
Flame holding without PJ ignitor	Marginal	Good
Without strut	Poor	Marginal
In weak comb. mode	Marginal	Fair
Combustion with parallel inj.	Poor	Good
Limit fuel rate for unstart	60 g/s	100 g/s

engine performance in an engine configuration with the 100-mm-long isolator and the 1/5H strut are compared in Table 2. In Table 2 "with preheating" means the self-ignition tests after engine combustion, therefore the engine has been heated by the burning of main fuel. "Without preheating" implies the engine condition when self-ignition was examined before the engine combustion. The results on the ignitability shows that the engine is near the self-ignition limit for both the S and V modes. However, the engine was found to self-ignite more easily in the V mode than in the S mode.

Flameholding characteristics also reflect the reactivity of the testing media. We tested the flameholding performance by turning off the PJ igniters after steady burning was attained. When the H_2 flow rate was high, turning off the igniters did not affect combustion in the S or V modes. However, when the bulk equivalence ratio Φ was low, turning off the igniters caused flameout of the top-wall pilot flame, and the main combustion sometimes decayed gradually in the S mode. Thus, turning off the igniters did not affect the flameholding in the V mode, but retarded it in the S mode.

In addition, the combustion with the normal injection was not possible in the S mode without the 1/5H strut. In the V mode, a modest thrust and combustion was observed in the engine configuration, even without the strut. The higher reactivity of the vitiated air is evident in these experiments.

B. Thrust and Combustion

The gross thrust in the S and V mode experiments are compared in Fig. 2 as functions of Φ, where corresponding fuel rates with $\Phi = 1$ is a fuel-flow rate of 153 g/s for the S and V modes. There are two combustion modes found in the figure: 1) the lower thrust mode up to about $\Phi = 0.33$ (weak combustion) and 2) the higher thrust mode (intensive combustion) from $\Phi = 0.33$ to the limit flow rate that caused engine unstart.[12] In the weak combustion mode, the engine exhausted a faint plume from the nozzle, whereas a bright flame was observed in the intensive combustion mode. These two modes sometimes appeared for a given fuel flow rate, and hysteresis was found in some experiments.

The solid symbols show the thrust measured with a main-vertical (MV) injection in the S-mode air and in the V-mode air. Slightly higher thrust was observed in the S mode than in the V mode, from $\Phi = 0.26$ to 0.4. The change in burning behavior in the two airflows becomes apparent when we compare the limit fuel flow rates for the engine unstart. The engine easily fell to the unstart condition in the S mode. The maximum Φ for engine start in the S mode was found to be about $\Phi = 0.45$. On the other hand, the engine worked with a higher Φ of 0.65 and overcame the engine drag in the V mode (Fig. 2). The engine drag was measured to be 1060 N in the S mode air and 1120 N in the V mode airflow.

In Fig. 2, the open symbols represent the effect of the main-parallel (MP) injection, added to the MV injection. The effects of addition of MP in the V mode, shown by the open squares, were examined with the MV rate kept constant ($\Phi = 0.44$). The data of MP addition are aligned on the extended line from that of the pure MV injection. Hence, the MP injection in the V mode assisted combustion by the MV injection. The open circles in Fig. 2 illustrate effects of the MP injection added to a fixed MV ($\Phi = 0.31$) in the S mode. Figure 2 shows that the MV injection did not produce the intensive combustion, and the MP injection caused the blow-off of the flame accompanied with the weak combustion in the S mode.

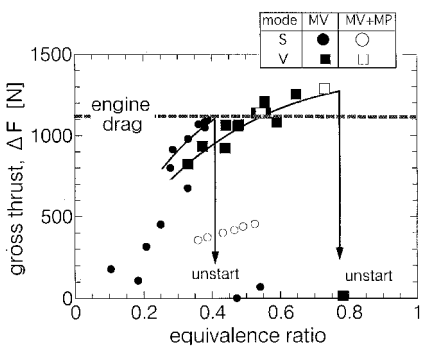

Fig. 2 Gross thrust against F in an engine configuration with the 100-mm-isolator and the 1/5-height strut: A fuel rate giving F = 1 is a fuel flow rate of 153 g/s for the S and V modes.

IV. Discussion

A. Premature Ignition with Radicals

The engine always autoignited without any ignition source in the V mode, which suggests promoted ignition by the residual radicals from the VAH. The shortened ignition delay time has been investigated by using the chemical kinetic code, designated as the one-dimensional kinetic (ODK) code.[1–5] Sato et al.[23] experimentally showed that the O_2 plasma–jet was most effective in igniting H_2/air mixtures in supersonic combustors. Mitani[5] explained why and how effective the O atom was in the H_2–O_2 system analytically.

Because the numerical calculations are not convenient to overview the fundamentals of phenomena, let us consider the ignition problem with a simplified analytical model consisting of a chain-initiation reaction: $H_2 + O_2 \rightarrow 2OH(R_6)$, and a branching reaction: $H + O_2 \rightarrow OH + O(R_1)$. Their characteristic times are $t_6 = [2k_6(O_2)]^{-1}$ and $t_1 = [k_1(O_2)]^{-1}$, respectively, where k_6 and k_1 are the rate constants of the two reactions.

The radical concentration is represented by X and the concentration of hydrogen is specified by X_{H_2}. Then the governing equation for X and the solution are given by

$$\frac{dX}{dt} = \frac{X}{t_1} + \frac{X_{H_2}}{t_6}, \quad X(0) = X_0 \tag{4}$$

$$X = X_0 \cdot \exp\left(\frac{t}{t_1}\right) + X_{H_2} \cdot \left(\frac{t_1}{t_6}\right) \cdot \left[\exp\left(\frac{t}{t_1}\right) - 1\right] \tag{5}$$

With the assumption that the critical radical concentration for ignition is X^*, the ignition delay can be calculated. The ignition delay, with an initial condition of $X_0 = 0$, is expressed as t_a. Normalization by the branching reaction time t_1, yields

$$\frac{t_a}{t_1} = \ell n\left[1 + \left(\frac{X^*}{X_{H_2}}\right) \cdot \left(\frac{t_6}{t_1}\right)\right] \tag{6}$$

Next, we define the ignition time with the radical addition ($X_0 \neq 0$) as t_b. The effect of the initial concentration of radicals is examined with the ratio t_b/t_a, as follows:

$$\frac{t_b}{t_a} = 1 - \left(\frac{t_1}{t_a}\right) \cdot \ell n\left[1 + \left(\frac{X_0}{X_{H_2}}\right) \cdot \left(\frac{t_6}{t_1}\right)\right] \tag{7}$$

Equation (7) indicates that the ignition delay time is strongly dependent on X_0, even for a small X_0, because of the large ratio of the two characteristic times, t_6/t_1. The effect of initial radical concentration becomes eminent as the inherent ignition delay time t_a becomes shorter in Eq. (7).

Figure 3 shows the promoted ignition by radicals, in which $X^* = 10^{-3}$ is assumed. The critical value of $X^* = 10^{-3}$ was chosen as follows. The first reason is that the total radical fraction approximately corresponds to the critical OH concentration of 5×10^{-9} mol/cc adopted in Ref. 2. The second reason is that the result on the promoted ignition is weakly dependent on the choice of X^*. The shortened ignition times are plotted against X^* with various temperatures. The broken line is a result obtained from the ODK calculation, where the O atom is introduced as a radical.[2] The agreement of the analytical result with the numerical result shows how well the

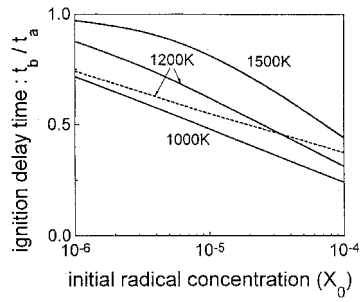

Fig. 3 Ignition promoted with radical addition. The critical radical concentration for ignition is assumed to be $X^* = 10^{-3}$.

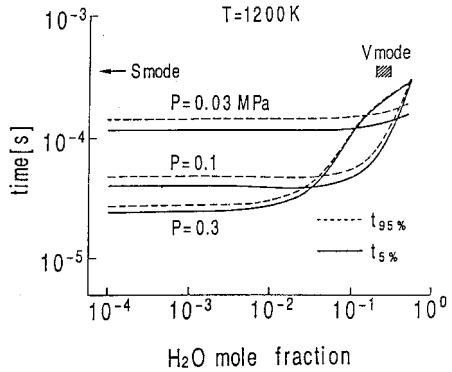

Fig. 4 H_2O inhibition effects to ignition delay time ($t_{5\%}$) and combustion time ($t_{95\%}$). The mole fractions of H_2O in the *S*- and *V*-modes air are indicated by the arrow and the shading.

simplified model approximates the full kinetics of H_2/air reactions.

For instance, the ignition time at 1500 K decreases by one-half with a radical mole fraction of 10^{-4}. The ignition accelerated by radicals can be expressed quantitatively as an equivalent temperature rise in test media. The ignition delay is governed by the R_1 with the activation temperature of 8200 K. To shorten the ignition delay time by one-half at 1500 K is equivalent to a temperature rise of 320 K. Namely, the testing with the vitiated air with $T_0 = 1500$ K is equivalent to the *S* mode with $T_0 = 1820$ K, if the vitiated air contains an initial radical concentration of 10^{-4} (100 ppm) from the VAH.

B. Inhibition Effect by H_2O

We evaluated the ignition and reaction times by using the ODK program. Figure 4 illustrates the ignition and reaction times as functions of the H_2O mole fraction. The definitions for these times are as in Ref. 3, namely, the ignition time is defined as the time taken to reach an ignition temperature (T_{ig}) from the initial temperature (T_i), that is, $T_{ig} = 0.05(T_{eq} - T_i) + T_i$, and denoted by $t_{5\%}$ in Fig. 4. The equilibrium temperature is denoted as T_{eq}. The total reaction time ($t_{95\%}$) is defined as the time it takes to reach a temperature $T_r = 0.95(T_{eq} - T_i) + T_i$ (which is expressed by the broken lines in Fig. 4). In Fig. 4, the H_2O range in the M6V and M8 modes in RJTF is indicated by shading. Because the air used is defrosted up to the dew point of 220 K, the H_2O concentration in the *S* mode is negligible, as shown by the arrow in Fig. 4.

The radical recombination process is affected by the reaction path: $H + HO_2 + M \rightarrow H_2 + O_2 + M$ in the ignition, where the third body is represented by *M*. The HO_2 reaction is greatly accelerated if the third body is H_2O because the third-body efficiency of H_2O is about 30 times greater than that of N_2. Therefore, the effect of vitiated air containing H_2O on engine testing has been investigated.

However, the reaction retarding effect does not appear in the low-pressure region, since the chain-breaking reaction is a termolecular reaction and the static pressure in the combustor of the engine is typically 25 kPa in the ignition stage. Hence, the retarding effect by H_2O is not important in the engine ignition. Only the premature ignition promoted by radicals appears in the ignition of the engine.

C. Autoignition and the Weak Combustion

The ignition time was calculated using the ODK code and compared with the flammable limit (the explosion peninsula[24]) of the stoichiometric H_2/air premixture in Fig. 5. The pressure range experienced in our scramjet engine is between 25 kPa (ignition) and 300 kPa (the intensive combustion). The static temperature is estimated to vary from 300 K in the core flow to 1450 K at the adiabatic wall. The possible reaction region, indicated by arrows in Fig. 5, is located to the right of the second explosion limit governed by the competition between the chain-branching reaction (R_1) and the HO_2 reaction discussed earlier. The opposite pressure dependence of ignition delay time, $dt_{5\%}/dP > 0$ in Fig. 4, is attributed to HO_2 recombination. The ignition time depends strongly on temperature, but it depends weakly on pressure near the flammability limit.

The flow velocity at the sonic point in the adiabatic boundary layer was evaluated to be 690 m/s, and the static temperature was 1260 K. Pitot pressure showed that the core flow speed was 1560 m/s, and the static temperature was 300 K in the engine exit without H_2 injection. The residence time of reactants in the engine becomes typically 1 ms in the core region of the engine. Decreasing the reaction temperature below 1000 K may make autoignition impossible in the engine, even under this infinitely fast mixing case. Comparison of the residence time with the ignition time shown in Fig. 5 indicates that the autoignition is possible only in the boundary layer developed on the engine wall.

We measured Φ and η_c distributions at the cross section of the engine exit with/without fuel injection to investigate the interaction between flowfield and combustion inside the engine. Detailed studies on the flowfield without fuel injection are found in Ref. 25, and the effects of struts attached in the combustor to mixing and combustion are reported in Ref. 26.

A typical $\Phi(z, y)$ distribution measured in the weak combustion is illustrated in Fig. 6a, when a low thrust of 129 N was measured with a total fuel of $\Phi = 0.30$. Although the fuel is supplied from uniformly distributed injection holes on the sidewalls, H_2 is concentrated near the top wall. No fuel exists near the cowl, and the H_2-lean region ($\Phi < 0.1$) covers almost all regions of the engine cross section. Because such a strong distortion is not found in a supersonic combustor with swept-back struts,[27] this may be because of the distorted airflow supplied from the swept-back inlet of the engine.

In addition to the vertical distribution, the mixing of H_2 in the spanwise direction is also limited in Fig. 6a. Hydrogen is confined to a narrow region near the sidewalls, especially around the corners with the top wall. Thus, mixing in the supersonic flow is so limited that H_2 injected in the combustor is trapped in the boundary layer on the walls.

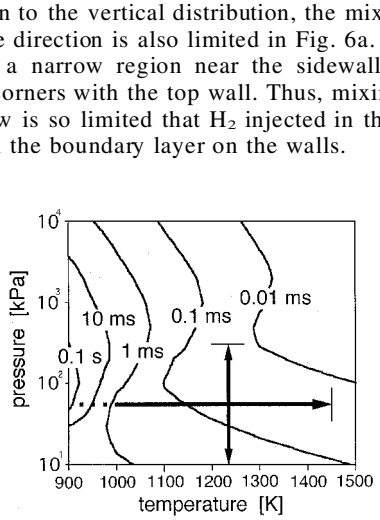

Fig. 5 Temperature and pressure dependence of ignition delay time ($t_{5\%}$). Reaction region in the scramjet engine is compared with the explosion peninsula of H_2/air mixture.

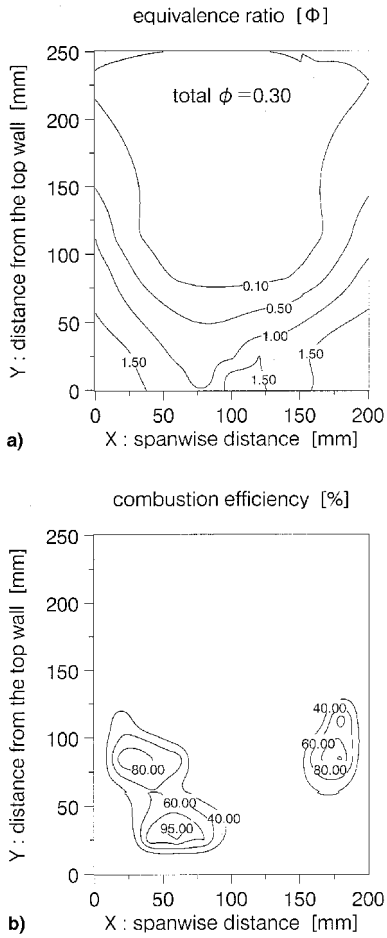

Fig. 6 a) Local equivalence ratio of H_2 and b) local combustion efficiency in the weak combustion mode (the *S*-mode experiment).

Figure 6b illustrates the local combustion efficiency in the weak combustion. Confined combustion regions were found near the sidewalls. Comparison with Fig. 6a indicates that the combustion takes place in the region with $0.5 < \Phi < 1.5$, and that the location of the highest combustion efficiency coincides in the region with $\Phi = 1$ in the boundary layer on the engine walls.

In the *V*-mode experiments, the engine could self-ignite without the igniters, and the weak combustion develop from it. In addition to the *V* mode, the weak combustion initiated downstream of the engine in the *S* mode. Thus, the weak combustion is the autoignition of the H_2 premixture trapped in the boundary layer. This kind of combustion has been observed by planar laser-induced fluorescence imaging of a transverse jet in a supersonic crossflow.[28]

Autoignition is achieved at a narrow margin, where the reaction time and the residence time are comparable, and it is only possible in the boundary layer. This is the reason why the ignitability was so strongly dependent on the test air and the engine temperature. The PJ igniters may assist ignition if the engine wall is cold, but it is not essential in a preheated engine condition. The weak combustion in the engine is not in the flameholding mode in which the flame propagation velocity and the flow velocity balance, but it results from flameholding by autoignition as observed in the flow reactor experiments.

D. Development to the Intensive Combustion Mode

The weak combustion mode switched to the intensive combustion as the fuel flow rate increased. Figure 7a is the Φ distribution in the intensive combustion, when the engine delivered an overall thrust of 1052 N with a total $\Phi = 0.42$. Although the distortion of H_2 in the vertical direction still remains, the distribution is flattened and the region with $\Phi < 0.2$ almost disappears in Fig. 7a.

In addition, the spanwise distribution is also improved with the intensive combustion. The fuel jet can penetrate deeper into the main flow in the intensive combustion because the higher the back pressure, the lower the pressure loss because of the overexpansion of the fuel jet. However, the increased penetration depth of the jet is not sufficient to explain the improved spanwise mixing. The mixing efficiency found in this engine testing is much higher than those in the experiments on wall injection by Chinzei et al.,[18] Murakami et al.,[29] and in the experiments on strut injection by Masuya et al.[30] This means that the distorted airflow from the inlet may interact with the combustion and produce separation bubbles on the sidewalls of the engine. Because the combustion fell in the weak mode without the struts, the attachment of the struts also accelerated the mixing of H_2 in the combustor. The dependence of flowfield on combustion is reported by Abbitt et al.[31]

Figure 7b shows the combustion efficiency measured in the intensive combustion mode, in which the engine exit is occupied by a region with a combustion efficiency higher than 80%, and the combustion is essentially complete. These improved mixing and combustion efficiencies produced the higher thrust performance in the intensive combustion mode.

To estimate the local heat flux to the engine, we monitored the engine wall temperature using thermocouples, embedded 1 mm deep from the inner surface at 40 stations. The development from the weak combustion mode to the intensive combustion mode can be observed from the variation of heat flux distribution in the engine measured in the *S*-mode air. The heat flux distributions along the centerline of the sidewall of the

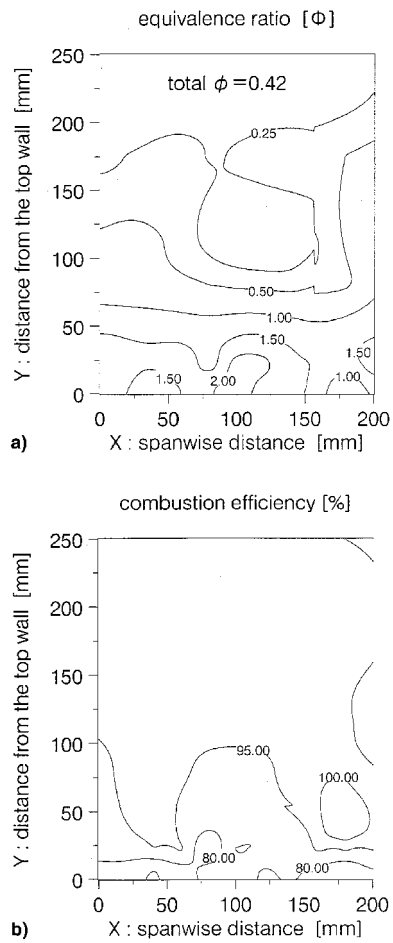

Fig. 7 a) Local equivalence ratio of H_2 and b) local combustion efficiency in the intensive combustion mode (the *S*-mode experiment).

engine, with the 200-mm-long isolator, is shown in Fig. 8a. In Fig. 8, the triangles represent the heat flux distribution before fuel injection. The first exothermic reaction, with a fuel flow rate of 30 g/s, appeared at the downstream part of the combustor (x = 1400 mm), where the shock wave from the cowl impinges. Note that there was no heating rate increase behind the step in the combustor from 800 to 900 mm. As the fuel flow rate increased from 30 to 48 g/s, the heating rate increased and the maximum point moved upstream. When the intensive combustion was attained at 70 g/s, the combustion was held at the step on the sidewall. Thus, the combustion is initiated downstream of the combustor rather than the vicinity of the step, as designed.

The heat flux distribution on the top wall (Fig. 8b) revealed another interesting variation with the fuel flow rate. The heating rate without H_2 injection (triangles) was low at about 0.2 MW/m^2. When a small amount of H_2 (21 g/s) was injected, the heat flux behind the step (x = 800 mm) increased four times. However, the heating rate at the nozzle exit was not affected so strongly. The heating rate on the top wall is lower and uniform, and it is insensitive to the fuel flow rate. These experimental facts imply that the exothermic reaction taking place on the top wall is weak and that the major exothermic reaction occurs on the sidewall in the divergent part of the engine.

However, the heating rate behind the top wall step suddenly decreased, when the intensive combustion was attained at 70 g/s. The flame on the top wall seemed to be blown off from the step, and stabilized downstream near x = 1500 mm. Detailed heat flux study in the engine clearly showed that the flame was anchored at the step on the sidewall, but near the cowl.[15] Thus, major heat release disappeared near the step on the top wall in the intensive combustion mode. Because the jet flame near the step suffers from insufficient mixing time[31] and strong turbulent strain,[32] it tends to blow off from the step.

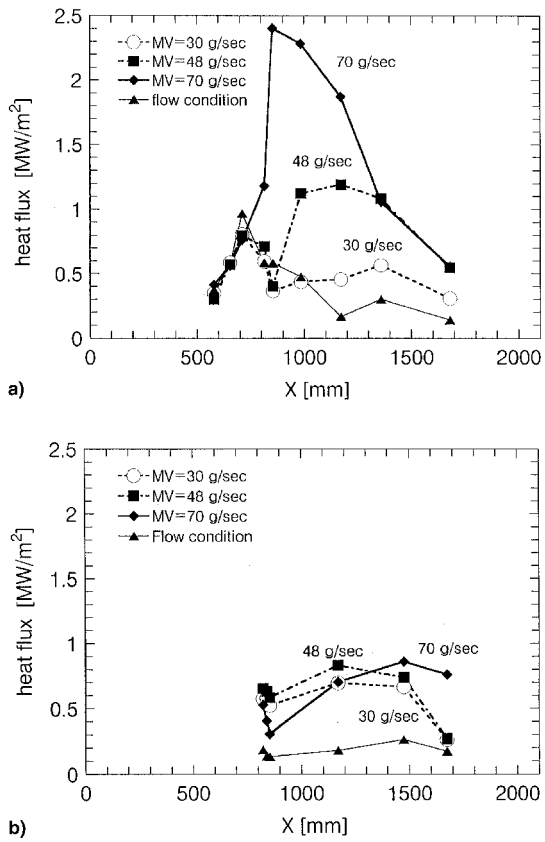

Fig. 8 Local heating rate on the a) sidewall and b) top wall found in an engine configuration with the 200-mm isolator with the 5/5-height strut.

The transition from the weak combustion mode to the intensive combustion mode occurred gradually as the fuel flow rate increased. We can elucidate the development in the wall pressure distributions in Fig. 9, which illustrates the pressure distributions measured on the top wall. In Fig. 9, the locations of isolator, combustion chamber, and the diverging combustor section are respectively denoted by Is., C.C., and D.C. on the x axis. The wall pressure is normalized by the total pressure in the facility nozzle reservoir. The bottom line denotes the pressure distribution in the engine without the fuel injection. The wall pressure increases in the inlet section up to 600 mm and decreases in the combustor and the divergence section. The maximum pressure is located at the exit of the inlet at x = 600 mm.

With the fuel flow rate of 45 g/s, a high-pressure region appeared downstream of the combustor at x = 1300 mm. It moved upstream as the fuel flow rate increased. However, the pressure rise caused by combustion is not experienced behind the step at MV = 45 g/s. The pressure pattern suggests that the principal exothermic region was stationed farther downstream of the step in the combustor. As the fuel flow rate increased, the precombustion shock wave reached the step, and it was trapped there up to the limit value at which the engine fell to the unstart.

E. Kinetically Controlled Combustion

The detached flame in the combustor is the key to understanding the sensitivity to the test air in the intensive combustion mode. The combustion region detached from the step was found in the V mode experiments. Figure 10 compares the wall pressure distributions measured on the top wall in the S and V modes with the same fuel flow rate (MV = 40 g/s). In Fig. 10, the pressure rise is found in the middle of the divergent part

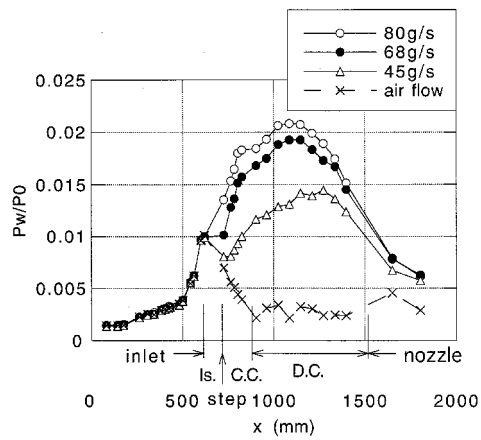

Fig. 9 Pressure distribution on the top wall of an engine with the 100-mm isolator with the 1/5-height strut.

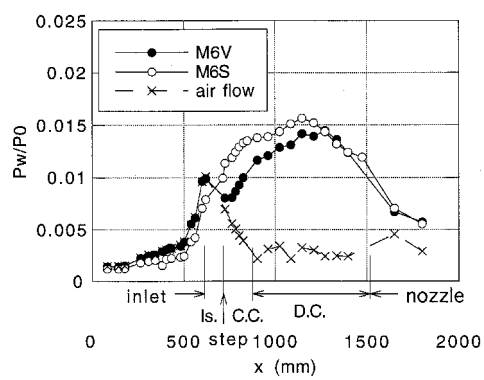

Fig. 10 Comparison of wall pressure between the V and the S modes (an engine with the 100-mm isolator with the 1/5-height strut).

of the combustor in the *V* mode, whereas it is at the entrance of the divergent part of the combustor in the *S* mode. Thus, the main combustion region shifts downstream in the *V* mode, and this shift explains the lower thrust performance found in the *V*-mode air between $\Phi = 0.26-0.4$ in Fig. 2.

Then, the next question is the mechanism of how the vitiated air decelerates combustion in the intensive combustion mode. The effect of H_2O appears as shown in Fig. 4 if the reaction pressure exceeds 100 kPa. In the intensive combustion mode, the combustor maintains a high pressure from 100 to 300 kPa. Therefore, the effect of H_2O can appear in the intensive combustion mode, but only if the combustion is kinetically controlled.

In addition, if the flame is held with recirculation-containing combustion products, the excess amounts of H_2O are supplied from the burnt region and the effect of the H_2O in the test air is hidden. The kinetically controlled combustion is possible, only if the flame is isolated from the separation bubbles. Thus, the kinetically controlled combustion is attributed to the detached flame developing from the autoignition.

The weak combustion mode near the top wall coexists with the intensive combustion mode. Increased pressure retards the combustion, and the main combustion region on the top wall shifts downstream in the *V* mode. Because H_2 mass flux is concentrated in the vicinity of the top wall, the incomplete combustion there drops the bulk combustion efficiency of the engine. This is the reason why the engine operated to $\Phi = 0.65$ in the *V* mode; in spite of that, the engine fell to unstart at $\Phi = 0.4$ in the *S* mode.

An example of strong interaction between the fluid dynamics and chemical kinetics is found in a numerical study,[33] where the HO_2 reaction governs thermal choking of a Mach 2 combustor. Although the high sensitivity of flowfield to kinetics might be originated from the numeric, the possibility of the kinetically controlled combustion should be investigated. The comparative studies of scramjet performance conducted in the NASA Langley Research Center's test complex raise the issues, namely, where the flame is held and whether the combustion is mixing controlled.[9] The presence of the combustion detached from the step found here seems to be responsible for the kinetically controlled phenomenon and answers the questions.

V. Conclusions

To investigate the sensitivity of scramjet engine performance to test air, an H_2-fueled engine was tested in the *S*- and *V*-mode air in the Mach 6 flight condition. The comparative study leads to the following conclusions:

1) Vitiated air showed artificially higher ignition performance in the scramjet engine. The engine could operate with $\Phi = 0.65$ in the *V* mode, but fell to the engine unstart condition above $\Phi = 0.4$ in the *S* mode.

2) The easier ignition in the vitiated air is caused by radicals supplied from the VAH. The premature ignition effect caused by the residual radical was expressed by an equivalent temperature increase of test air.

3) Distributions of heat flux and wall pressure showed that the weak combustion mode is a phenomenon resulting from autoignition. The distributions of H_2 and combustion efficiency in the weak combustion mode also suggested the autoignition in the boundary layer developed on the engine wall.

4) In the intensive combustion mode, a flame was held at the backward-facing step in the combustor. The gas sampling showed that the flowfield in the engine was drastically changed and mixing in the engine was greatly improved by combustion.

5) The detached flame coexists with the anchored flame in the intensive combustion mode. The inhibition by H_2O can affect the detached flame to deteriorate the combustion performance of a scramjet. The detached flames may produce the kinetically controlled combustion and the sensitivity of thrust performance to the test air.

Acknowledgment

This study was conducted as a part of the National Aerospace Laboratory—Mitsubishi Heavy Industries, Ltd., cooperative research.

References

[1]Bahn, G. S., "Calculations on the Autoignition of Mixtures of Hydrogen and Air," NASA CR 112067, April 1972.

[2]Carson, G. T., Jr., "Analytical Chemical Kinetic Investigation of the Effects on Oxygen, Hydrogen, and Hydroxyl Radicals on Hydrogen-Air Combustion," NASA TN-D7769, Sept. 1974.

[3]Rogers, R. C., and Schexnayder, C. J., Jr., "Chemical Kinetic Analysis of Hydrogen-Air Ignition and Reaction Times," NASA TP 1856, July 1981.

[4]Jachimowski, C. J., "An Analytical Study of the Hydrogen-Air Reaction Mechanism with Application to Scramjet Combustion," NASA TP-2791, Feb. 1988.

[5]Mitani, T., "Ignition Problems in Scramjet Testing," *Combustion and Flame*, Vol. 101, 1995, pp. 347–359.

[6]Suttrop, F., "Comment on Experimental Study on Autoignition in a Scramjet Combustor," *Journal of Propulsion and Power*, Vol. 8, No. 6, 1992, pp. 1300–1302.

[7]Northam, G. B., "Report on Combustion in Supersonic Flow," *Proceedings of the 21st JANNAF Combustion Meeting*, Chemical Propulsion Information Agency, 1984, pp. 399–410.

[8]Srinivasan, S., and Erickson, W., "Interpretation of Vitiation Effects on Testing at Mach 7," AIAA Paper 95-2719, July 1995.

[9]Guy, R. W., Rogers, R. C., Puster, R. L., Rock, K. E., and Diskin, G. S., "The NASA Langley Scramjet Test Complex," AIAA Paper 96-3243, July 1996.

[10]Hiraiwa, T., Mitani, T., Izumikawa, M., and Ono, F., "Calibration of Nozzle Flow in Ramjet Engine Test Facility," 20th International Symposium on Space Technology and Science, 96-d-14, May 1994.

[11]Yatsuyanagil, N., Chinzei, N., and Miki, Y., "Initial Tests of a Sub-Scale Scramjet Engine," 12th ISABE, Melburne, Australia, Sept. 1995.

[12]Kanda, T., Saito, T., Komuro, T., Ono, F., and Matsui, A., "M6 Testing of a Scramjet Engine Model," AIAA Paper 96-0380, Jan. 1996.

[13]Tomioka, S., Hiraiwa, T., Sakuranaka, N., Murakami, A., and Matsui, A., "Ignition Strategy in a Model Scramjet," AIAA Paper 96-3240, July 1996.

[14]Saito, T., Wakamatsu, Y., Mitani, T., Chinzei, N., and Shimura, T., "Mach 8 Testing of a Scramjet Engine Model," 20th International Symposium on Space Technology and Science, 96-a-2-11, May 1996.

[15]Hiraiwa, T., Sato, S., Tomioka, S., and Kanda, T., "Testing of a Scramjet Engine Model in Mach 6 Vitiation Air Flow," AIAA Paper 97-0292, Jan. 1997.

[16]Mitani, T., Ueda, S., Tani, K., Sato, S., Miyajima, H., Matsumoto, M., and Yasu, S., "Validation Studies of Scramjet Nozzle Performance," *Journal of Propulsion and Power*, Vol. 9, No. 5, 1993, pp. 725–730.

[17]Anderson, G. Y., and Gooderum, P. B., "Exploratory Tests of Two Strut Fuel Injectors for Supersonic Combustion," NASA TN D-7581, Feb. 1974.

[18]Chinzei, N., Komuro, T., Kudou, K., Murakami, A., Tani, K., Masuya, G., and Wakamatsu, Y., "Effects of Injector Geometry on Scramjet Combustor Performance," *Journal of Propulsion and Power*, Vol. 1, No. 1, 1993, pp. 146–152.

[19]Eggers, J. M., Reagon, P. G., and Gooderum, P. B., "Combustion of Hydrogen in a Two-Dimensional Duct with Step Fuel Injectors," NASA TP-1159, April 1978.

[20]McClinton, C. R., "Interaction Between Step Fuel Injectors on Opposite Walls in a Supersonic Combustor Model," NASA TP 1174, March 1978.

[21]Waitz, I. A., Marble, F. E., and Zukoski, E. E., "Investigation of a Contoured Wall Injector for Hypervelocity Mixing Augmentation," *AIAA Journal*, Vol. 31, No. 6, 1993, pp. 1014–1021.

[22]Mitani, T., "Quenching of Reaction in Gas Sampling Probes to Measure Scramjet Engine Performance," 26th International Symposium on Combustion, Naples, July 1996.

[23]Sato, Y., Sayama, M., Masuya, G., Komuro, T., Kudou, K., Murakami, A., Tani, K., and Chinzei, N., "Experimental Study on Autoignition in a Scramjet Combustor," *Journal of Propulsion and Power*, Vol. 8, No. 4, 1992, p. 883.

[24]Lewis, B., and Von Elbe, G., *Combustion, Flames and Explosions*

of Gases, 2nd ed., Academic, New York, 1961, pp. 22–70.

[25]Tani, K., Kanda, T., Sunami, T., Hiraiwa, T., and Tomioka, S., "Geometrical Effects to Aerodynamic Performance of Scramjet Engine," AIAA Paper 97-3018, July 1997.

[26]Sato, S., Izumikawa, M., Tomioka, S., and Mitani, T., "Scramjet Engine Test at the Mach 6 Flight Condition," AIAA Paper 97-3021, July 1997.

[27]McClinton, C. R., Torrence, M. G., Gooderum, P. B., and Young, I. G., "Nonreactive Mixing Study on a Scramjet Swept-Strut Fuel Injector," NASA TN D-8069, Dec. 1975.

[28]Lee, M. P., McMillin, B. K., Palmer, J. L., and Hanson, R. K., "Planar Fluorescence Imaging of a Transverse Jet in a Supersonic Crossflow," *Journal of Propulsion and Power*, Vol. 8, No. 4, 1992, pp. 729–735.

[29]Masuya, G., Komuro, T., Murakami, A., Shinozaki, N., Nakamura, A., Murayama, M., and Ohwaki, K., "Ignition and Combustion Performance of Scramjet Combustor with Fuel Injection Struts," *Journal of Propulsion and Power*, Vol. 11, No. 2, 1995, pp. 301–307.

[30]Murakami, A., Komuro, T., and Kudo, K., "Experiment on a Rectangular Cross Section Scramjet Combustor (II), Effects of Fuel Injector Geometry," National Aerospace Lab., TR-1220, 1993 (in Japanese).

[31]Abbitt, J. D., III, Segal, C., McDaniel, J. C., Krauss, R. H., and Whitehead, R. B., "Experimental Supersonic Hydrogen Combustion Employing Staged Injection Behind a Rearward-Facing Step," *Journal of Propulsion and Power*, Vol. 9, No. 3, 1993, pp. 472–478.

[32]Balakrishnan, G., and Williams, F. A., "Turbulent Combustion Regimes for Hypersonic Propulsion Employing Hydrogen-Air Diffusion Flames," *Journal of Propulsion and Power*, Vol. 10, No. 3, 1994, pp. 434–437.

[33]Segal, C., McDaniel, J. C., Whitehurst, R. B., and Krauss, R. H., "Mixing and Chemical Kinetic Interactions in a Mach 2 Reacting Flow," *Journal of Propulsion and Power*, Vol. 11, No. 2, 1995, pp. 308–314.